Energy & Environmental Science

ROYAL SOCIETY OF CHEMISTRY

COMMUNICATION

View Article Online
View Journal | View Issue

Check for updates

Cite this: *Energy Environ. Sci.*, 2021, **14**, 2263

Received 8th December 2020,
Accepted 23rd February 2021

DOI: 10.1039/d0ee03839c

rsc.li/ees

22.8%-Efficient single-crystal mixed-cation inverted perovskite solar cells with a near-optimal bandgap†

Abdullah Y. Alsalloum, ‡[a] Bekir Turedi, ‡[a] Khulud Almasabi, ‡[a] Xiaopeng Zheng,[a] Rounak Naphade,[a] Samuel D. Stranks, [bc] Omar F. Mohammed[a] and Osman M. Bakr *[a]

Expanding the near-infrared (NIR) response of perovskite materials to approach the ideal bandgap range (1.1–1.4 eV) for single-junction solar cells is an attractive step to unleash the full potential of perovskite solar cells (PSCs). However, polycrystalline formamidinium lead triiodide ($FAPbI_3$)-based absorbers, used in record-efficiency PSCs, currently offer the smallest bandgap that can be achieved for lead-halide perovskite thin films (>100 meV larger than the optimal bandgap). Here, we uncover that utilizing a mixed-cation single-crystal absorber layer ($FA_{0.6}MA_{0.4}PbI_3$) is capable of redshifting the external quantum efficiency (EQE) band edge past that of $FAPbI_3$ polycrystalline solar cells by about 50 meV – only 60 meV larger than that of the top-performing photovoltaic material, GaAs – leading to EQE-verified short-circuit current densities exceeding 26 mA cm^{-2} without sacrificing the open-circuit voltage (V_{OC}), and therefore, yielding power conversion efficiencies of up to 22.8%. These figures of merit not only set a new record for SC-PSCs and are among the highest reported for inverted-structured-PSCs, but also offer an avenue for lead halide PSCs to advance their performance toward their theoretical Shockley–Queisser Limit potential.

Broader context

Solar cells based on lead halide perovskites (PSCs) have recently emerged as cost-effective and energy-efficient candidates to replace or complement established photovoltaic technologies such as Silicon and GaAs. In such technologies, single crystals have led the way in terms of efficiency, performing better than their polycrystalline counterparts because of their lower defect density. However, the pace progress of single-crystal PSCs (SC-PSCs) has been very slow in comparison with that of polycrystalline PSCs partly because of challenges in crystal growth and device integration. High-efficiency PSCs utilize polycrystalline formamidinium lead triiodide ($FAPbI_3$)-based absorbers, which provide the smallest achievable bandgap for lead-halide perovskite thin films, yet are still more than 100 meV larger than the optimal bandgap range for single-junction solar cells (1.1–1.4 eV). In this work, we successfully incorporate a mixed-cation single-crystal absorber layer ($FA_{0.6}MA_{0.4}PbI_3$) and show, without compromising on open circuit voltage, that the near infrared response of the devices can be expanded beyond those of polycrystalline $FAPbI_3$ by about 50 meV, which brings it close to that of the best-performing photovoltaic semiconductor, GaAs. As a result, we achieve short circuit current values of more than 26 mA cm^{-2} and conversion efficiencies of up to 22.8%, which sets a new record for SC-PSCs.

Due to their exceptional optoelectronic properties and ease of processing, metal halide perovskites – with the general formula of ABX_3 where A is the cation, B is the metal and X is the halide – have become, arguably, the most studied class of semiconductors during the past decade.[1] Rapid developments in the field yielded solar cells, light emitting diodes and various types of photodetectors that are competing head-to-head with the state-of-the-art optoelectronic devices.[1–8] Lead halide perovskite solar cells (PSCs), the leading perovskite technology, are primarily based on polycrystalline films and have already achieved outstanding power conversion efficiencies (PCEs) surpassing well-established photovoltaic technologies such as cadmium telluride (CdTe) and copper indium gallium selenide (CIGS).[9,10]

Of the standard cations (formamidinium (FA^+), methylammonium (MA^+), and cesium (Cs^+)) and halides (I^-, Br^-, Cl^-) comprising perovskite films, the best PSCs favor FA and I since they offer better thermal/operational stability and a smaller bandgap that is closer – but not there yet – to the ideal Shockley Queisser Limit (SQL) range for single-junction solar cells (1.1–1.4 eV).[11–15] The best single-junction solar cells are made of single-crystal Gallium Arsenide (GaAs, η = 29.1%), which has a bandgap of around 1.4 eV.[9] This suggests that reducing the

[a] *Division of Physical Sciences and Engineering, King Abdullah University of Science and Technology, Thuwal 23955-6900, Kingdom of Saudi Arabia. E-mail: osman.bakr@kaust.edu.sa*
[b] *Cavendish Laboratory, University of Cambridge, JJ Thomson Avenue, Cambridge CB3 0HE, UK*
[c] *Department of Chemical Engineering and Biotechnology, University of Cambridge, Philippa Fawcett Drive, Cambridge CB3 0AS, UK*

† Electronic supplementary information (ESI) available. See DOI: 10.1039/d0ee03839c

‡ Abdullah Y. Alsalloum, Bekir Turedi and Khulud Almasabi contributed equally to this work.

absorber layer bandgap while maintaining the high crystal quality is paramount for further enhancing the performance of PSCs toward their theoretical potential. One adopted strategy to lower the bandgap is to alloy Pb with Sn; however, this composition sacrifices the crystal quality and stability of the films because of the high density of intrinsic defect species – Sn vacancies – attributed to the oxidation of Sn^{2+} to Sn^{4+} when exposed to air and the solvents used to fabricate the films.[16] Another approach is to use a thicker single-crystal absorber instead of the standard polycrystalline film to extend the spectral response.[17–19] Thus far, all the high efficiency ($\gtrapprox$20%) single-crystal perovskite solar cells (SC-PSCs) are based on $MAPbI_3$ and have achieved efficiencies of up to 21.9%.[19,20] However, the bandgap of $MAPbI_3$ single-crystal films is markedly larger than the ideal SQL range for single-junction solar cells, and also wider than that of $FAPbI_3$ polycrystalline films.

Here, we reveal that utilizing a micron-thick mixed cation single-crystal absorber layer is capable of effectively red-shifting the external quantum efficiency (EQE) band edge past that of pure $FAPbI_3$ polycrystalline films, resulting in J_{sc} values exceeding 26 mA cm^{-2} and PCEs of up to 22.8%, which are among the highest values achieved in devices of the inverted architecture. Compared with polycrystalline films, perovskite single crystals possess lower defect densities and longer charge carrier diffusion lengths,[21–24] which, in turn, allows for thicker absorber layers to be incorporated, thereby, significantly enhancing light absorption at the band edge. These results not only set a record for SC-PSCs, but also provide a strategy to engineer PSC performance toward that of GaAs solar cells.

Fig. 1a illustrates the implication of a bandgap redshift on the theoretical performance limit of single-junction solar cells. Lying almost at the peak of the SQL curve, single-crystal GaAs solar cells provide a theoretical maximum PCE of about 32.9% corresponding to a theoretical J_{SC} of 31.8 mA cm^{-2}, whereas polycrystalline $FAPbI_3$ cells offer a theoretical PCE of approximately 31.6% with a J_{SC} of 27.8 mA cm^{-2}. Bridging this >1% gap in PCE might prove to be the key for PSCs to match, if not surpass, the leading photovoltaic performer. We found that mixed-cation SC-PSCs are positioned in between these two semiconductor devices; the SQL PCE is about 32.3% corresponding to a J_{SC} of 29.8 mA cm^{-2}.

The mixed cation single-crystal thin films were grown directly on the hole transporting layer, poly(triaryl amine) (PTAA), in the solvent γ-butyralactone (GBL) using the space-limited inverse temperature crystallization method (see the ESI† for experimental details).[17,26,27] PTAA serves as a suitable transporting layer compatible with this growth method due to its hydrophobicity, which facilitates the diffusion of perovskite-solvent complexes leading to more favorable growth of the crystal films. Initially, we experimented with different ratios of FA to MA to grow $FA_xMA_{1-x}PbI_3$ films, where x = 0.6, 0.8 and 1. For each ratio, we tuned the solution concentration such that crystallization was initiated at 70 °C. As expected for x = 1, crystals in the form of yellow rods emerged, indicating the formation of the non-perovskite phase typical of FA rich compositions. For x = 0.8, yellow rods also appeared along with

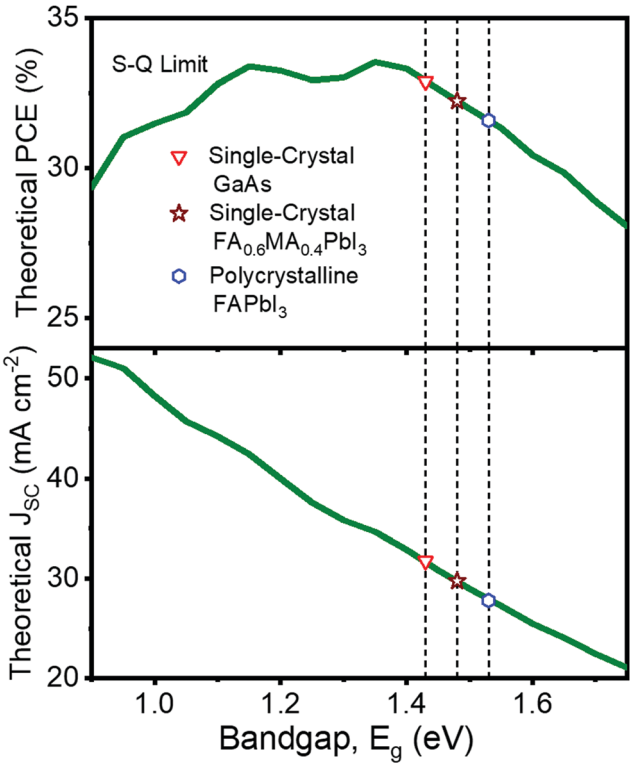

Fig. 1 The Shockley–Queisser theoretical limit for the power conversion efficiency (PCE) and short-circuit current density (J_{SC}) of single-junction solar cells as a function of the bandgap. Note that the literature bandgap value of $FAPbI_3$ varies from 1.45 to 1.55 eV depending on the method used to calculate the bandgap. Here, the dashed lines represent the bandgap as calculated from the inflection point of the device external quantum efficiency spectrum, where the value of single-crystal GaAs was obtained from ref. 25 and that of polycrystalline $FAPbI_3$ was obtained from ref. 11 and confirmed in this work.

irregular-shaped black crystals (ESI,† Fig. S3). For x = 0.6, only the black perovskite phase was observed in the form of rhomboidal- or hexagonal-shaped crystals similar to that of $MAPbI_3$, resulting in large-area films suitable for device fabrication and characterization. Therefore, $FA_{0.6}MA_{0.4}PbI_3$ was chosen as the composition of choice in this work. X-ray diffraction (XRD) of the films revealed only two peaks corresponding to the (110) and (220) planes of the cubic perovskite structure (ESI,† Fig. S4a), indicating that the preferred growth orientation of the single-crystal films was the (110) orientation. The cubic structure can be differentiated from the tetragonal one typical of MA rich compositions by checking the absence of the tetragonal (211) peak at ~23.5° in the powder XRD pattern of the ground crystal films (ESI,† Fig. S4b).[17,28] To discern the ratio of FA to MA in the films compared with that in the precursor solution, proton nuclear magnetic resonance (^{1}H-NMR) was conducted (ESI,† Fig. S5) and a ratio of 63% : 37% of FA^+ : MA^+ was determined from the NMR spectrum (herein denoted as $FA_{0.6}MA_{0.4}$), close to the initial precursor composition with a very slight shift toward FA. This small shift likely stems from the lower solubility of the FA perovskite in GBL.[29]

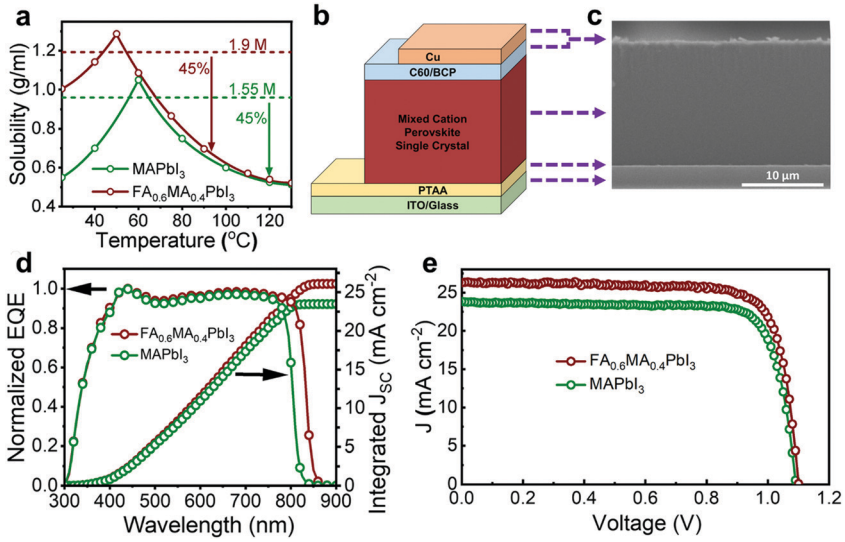

Fig. 2 (a) Temperature-dependent solubility of $FA_{0.6}MA_{0.4}PbI_3$ and $MAPbI_3$ in GBL. The horizontal dashed lines represent the starting concentration of the precursor solution. (b) Device architecture of the single-crystal device. (c) Cross-sectional SEM image of the single-crystal cell. Note that the few nanometer-thick transporting layers are not visible at such magnifications. (d) EQE spectra and (e) *J*–*V* curve comparison between single-crystal $MAPbI_3$ and $FA_{0.6}MA_{0.4}PbI_3$ devices. All measurements were conducted under 1-sun illumination.

Fig. 2a shows the solubility of $FA_{0.6}MA_{0.4}PbI_3$ and $MAPbI_3$ in GBL as a function of temperature. Compared with $MAPbI_3$, which has a maximum solubility of about 1.7 M at 60 °C, $FA_{0.6}MA_{0.4}PbI_3$ has a maximum of 2.1 M at around 50 °C. The difference in the solubility behavior, particularly at lower temperatures, can be attributed to the ability of FA to solubilize PbI_2 more effectively compared with that of MA. This allows us to dissolve more of the perovskite, which ultimately results in a greater precipitation quantity at higher temperatures and larger area films. Moreover, the use of FA enables crystallization to occur at lower temperatures, which has been previously shown to yield devices with better V_{OC} values, especially when involving the volatile cation MA.[19] The nucleation temperatures of $FA_{0.6}MA_{0.4}PbI_3$ and $MAPbI_3$ are around 70 °C and 100 °C for solution concentrations of 1.9 M and 1.55 M, respectively. The temperature is then further increased to promote growth of the single-crystal films.

Inverted p–i–n planar solar cells from the single-crystal films were constructed and tested under 1-sun illumination. The device structure consists of ITO/PTAA/$FA_{0.6}MA_{0.4}PbI_3$/C_{60}/Bathocuproine (BCP)/Cu (Fig. 2b). A cross-sectional scanning electron microscopy (SEM) image of the device is presented in Fig. 2c, showing a ~15 μm-thick single-crystal absorber layer. The increase in PCE compared with the previously reported high efficiency SC-PSCs based on $MAPbI_3$ stems from the increase in the J_{SC} from about 24 to 26 mA cm^{-2}. This can better be seen by looking more closely at a comparison between the EQE spectra of $MAPbI_3$ and $FA_{0.6}MA_{0.4}PbI_3$ (Fig. 2d). As shown, a clear redshift in the band edge by approximately 30 nm occurs due to the reduction in bandgap, which can also be seen in the steady-state absorption spectra of the $FA_{0.6}MA_{0.4}PbI_3$ and $MAPbI_3$ single-crystal films (Fig. S7, ESI†). As a result, about a 2 mA cm^{-2} jump in the integrated current density takes place. Since the bandgap is reduced, one would expect the V_{OC} to decrease, which is, surprisingly, not the case; the V_{OC} values compared with those of $MAPbI_3$-based devices prepared with the same solvent (GBL) are almost similar (Fig. 2e).[17] However, the achieved V_{OC} values are lower than those of $MAPbI_3$-based devices prepared at lower temperatures as detailed in our previous work.[19] This suggests that either or both of the following two factors could be at play. First, the introduction of FA changes the solubility behavior, enabling a reduction in the crystallization temperature, as described earlier, which has been shown to generate a higher V_{OC} by limiting the escape of MAI. Second, FA is more thermally stable and less volatile than MA, and is thus, less affected by higher temperature processes needed to carry out crystallization, resulting in a less defective structure. It is worth noting that no passivation treatment was conducted to fabricate the SC-PSCs, whereas nearly all highly efficient polycrystalline PSCs rely on surface and grain-boundary passivation to boost the V_{OC}.[30–34]

The *J*–*V* characteristics of the best device are illustrated in Fig. 3a. A reverse-scan PCE, J_{SC}, open-circuit voltage (V_{OC}) and fill factor (*FF*) of 22.8%, 26.2 mA cm^{-2}, 1.1 V, and 0.79, respectively, were achieved with negligible hysteresis. The stabilized maximum power output (SPO) of the champion device was determined by holding the voltage at maximum power point (0.94 V) and recording the generated photocurrent (Fig. 3b). The SPO verifies the attained PCE with a stabilized value of ~22.5%, closely matching that of the *J*–*V* measurement. The superior J_{SC} was also confirmed by measuring the EQE (Fig. 3c). The integrated current-density amounts to a J_{SC} value of 26.1 mA cm^{-2}, similar to that obtained from the *J*–*V* curves. A statistical analysis of the photovoltaic parameters of 10 fabricated devices is displayed in Fig. 3d, revealing their good reproducibility.

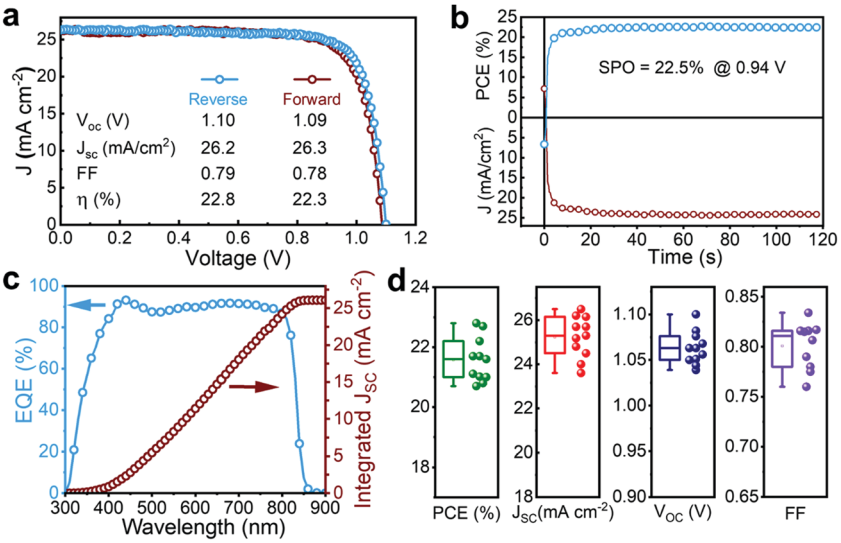

Fig. 3 (a) J–V curves of the best device under reverse (blue) and forward (red) scans. (b) Stabilized power output of the best cell at maximum power point with an applied bias of 0.94 V. (c) EQE spectrum and integrated J_{SC} of the best cell. (d) Statistical analysis of the photovoltaic parameters for 10 devices including PCE, V_{OC}, J_{SC} and FF. Measurement was conducted under 1-sun illumination.

It is constructive to compare the EQE spectrum of our mixed cation SC-PSCs to that of $FAPbI_3$-based polycrystalline PSCs since the record PSCs are primarily based on this composition. Fig. 4a shows a comparison among the EQE spectra of $FA_{0.6}MA_{0.4}PbI_3$ single-crystalline, $FA_{0.6}MA_{0.4}PbI_3$ polycrystalline, and $FAPbI_3$ polycrystalline devices fabricated with the same inverted device architecture. Remarkably, the $FA_{0.6}MA_{0.4}PbI_3$ SC-PSCs show a significantly greater redshift in the EQE band edge compared with that of $FAPbI_3$ polycrystalline cells. This means that SC-PSCs are capable of absorbing and utilizing the solar spectrum more effectively toward a higher theoretical limit.

Quantifying the exact bandgap of $FAPbI_3$ is a challenging task since the value varies depending on the method used to determine it, as detailed by Krückemeier *et al.*, who recently conducted a *meta*-analysis of such methods and proposed the use of the inflection point of the EQE, $E_g^{EQE,ip}$, as a general approach to determine the bandgap when referencing the SQL and solar cell performances.[35] Since the Shockley–Queisser model bases its approach on the external properties of the device rather than the internal characteristics of the absorber material, extracting the bandgap from the EQE spectrum is more reasonable in this context. Using this definition, we attempt to calculate $E_g^{EQE,ip}$ of our mixed-cation SC-PSCs and compare it with those of other standard compositions (Fig. 4b). $E_g^{EQE,ip}$ for the mixed-cation SC-PSCs yields a value of 1.48 eV, which is about 50 meV lower than that of $FAPbI_3$ polycrystalline devices (1.53 eV). Note that the value of $E_g^{EQE,ip}$ for our fabricated $FAPbI_3$ polycrystalline cells agrees well with that in the literature.[11–14,35,36]

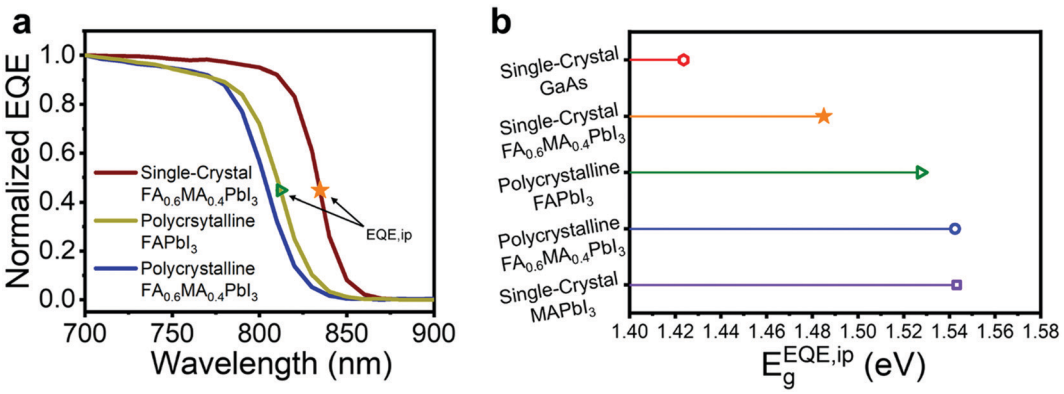

Fig. 4 (a) EQE spectra comparison between the single-crystal $FA_{0.6}MA_{0.4}PbI_3$ device and polycrystalline $FAPbI_3$ and $FA_{0.6}MA_{0.4}PbI_3$ devices with the same device architecture. (b) Bandgap of select absorber materials calculated from the inflection point of the EQE spectrum. The bandgap value for GaAs was obtained from ref. 25.

To assess the long-term stability, we conducted the following tests. First, we compared the thin film compositional stability of both polycrystalline and single-crystalline $MAPbI_3$ and mixed cation compositions at 85 °C and 65% relative humidity (Fig. S8, ESI†). As expected, the single-crystal films turned yellow days after their polycrystalline counterparts primarily because of the less surface area exposed in the grain-free single-crystal films. Moreover, the single-crystal mixed-cation composition showed a much better thermal stability compared with that of $MAPbI_3$ single-crystal films.

As such, we surmised that the thermal stability of the devices would follow the same trend. However, to our surprise, after heating the cells at 85 °C in a glovebox for one day, we found that the performance of the single-crystal devices dropped down significantly, which constituted a concern that required further investigation. After careful inspection, we discovered that the reason behind this dramatic loss in performance stemmed from the crystal films detaching from the ITO substrate, which could be seen by the naked eye. Fig. S9 (ESI†) shows an image of a 1 year-stored well-attached film and a thermally heated detached film. This issue likely originates from the stresses generated when heating, *i.e.* the difference in thermal expansion coefficients between the crystal film and substrate combined with the weak van der Waals bonding. This means that a rigid glass/ITO substrate is unlikely to be compatible with single-crystal films for long-term operational stability, and thus, future efforts should focus on eliminating the glass/transparent conductive oxide (TCO) part. One promising route that can both solve this problem and theoretically enhance the performance further is to exploit the long diffusion length of single crystal films to construct lateral solar cells, an area that is still underexplored in the field due to the short-diffusion length in grain-containing polycrystalline films. The long-diffusion length enables the effective deposition of tens-of-micrometers-separated electrodes on one side without short circuiting.[26,37,38] Moreover, eliminating the glass/TCO component eliminates the accompanying parasitic absorptions and reflections, thereby significantly enhancing light absorption and the J_{SC}.

In summary, mixed cation SC-PSCs were fabricated exhibiting PCEs of up to 22.8% and J_{SC} values exceeding 26 mA cm^{-2}, which are new record values for SC-PSCs and are among the highest for inverted p–i–n devices. The rise in performance mainly stemmed from an increase in J_{SC}, which was verified by EQE measurements with a significant redshift in the band edge. This redshift was even more pronounced than that of $FAPbI_3$ polycrystalline solar cells, which provides a pathway for lead halide perovskites to approach the absorption characteristics of the star photovoltaic semiconductor, single-crystalline GaAs. Suggested future efforts include interface engineering and exploration of SC-PSCs in more favorable architectures such as lateral structures.

Conflicts of interest

The authors declare no competing financial interests: S.D.S. is a co-founder of Swift Solar. O.M.B. is a founder of Quantum Solutions (Qdot.inc).

Acknowledgements

We acknowledge the use of KAUST Core Lab and KAUST Solar Center facilities. S.D.S acknowledges the Royal Society and Tata Group (UF150033).

References

1 A. K. Jena, A. Kulkarni and T. Miyasaka, Halide Perovskite Photovoltaics: background, Status, and Future Prospects, *Chem. Rev.*, 2019, **119**, 3036–3103.
2 G. Kakavelakis, M. Gedda, A. Panagiotopoulos, E. Kymakis, T. D. Anthopoulos and K. Petridis, Metal Halide Perovskites for High-Energy Radiation Detection, *Adv. Sci.*, 2020, **7**, 2002098.
3 K. Lin, J. Xing, L. N. Quan, F. P. G. de Arquer, X. Gong, J. Lu, L. Xie, W. Zhao, D. Zhang, C. Yan, W. Li, X. Liu, Y. Lu, J. Kirman, E. H. Sargent, Q. Xiong and Z. Wei, Perovskite light-emitting diodes with external quantum efficiency exceeding 20 per cent, *Nature*, 2018, **562**, 245–248.
4 P. Wangyang, C. Gong, G. Rao, K. Hu, X. Wang, C. Yan, L. Dai, C. Wu and J. Xiong, Recent Advances in Halide Perovskite Photodetectors Based on Different Dimensional Materials, *Adv. Opt. Mater.*, 2018, **6**, 1701302.
5 H. Tsai, W. Nie, J. C. Blancon, C. C. Stoumpos, C. M. M. Soe, J. Yoo, J. Crochet, S. Tretiak, J. Even, A. Sadhanala, G. Azzellino, R. Brenes, P. M. Ajayan, V. Bulovic, S. D. Stranks, R. H. Friend, M. G. Kanatzidis and A. D. Mohite, Stable Light-Emitting Diodes Using Phase-Pure Ruddlesden-Popper Layered Perovskites, *Adv. Mater.*, 2018, **30**, 1704217.
6 S. A. Veldhuis, P. P. Boix, N. Yantara, M. Li, T. C. Sum, N. Mathews and S. G. Mhaisalkar, Perovskite Materials for Light-Emitting Diodes and Lasers, *Adv. Mater.*, 2016, **28**, 6804–6834.
7 S. Das, S. Gholipour and M. Saliba, Perovskites for Laser and Detector Applications, *Energy Environ. Mater.*, 2019, **2**, 146–153.
8 X. Zheng, A. Y. Alsalloum, Y. Hou, E. H. Sargent and O. M. Bakr, All-Perovskite Tandem Solar Cells: a Roadmap to Uniting High Efficiency with High Stability, *Acc. Mater. Res.*, 2020, **1**, 63–76.
9 NREL Best Research-Cell Efficiency Chart, 2020https://www.nrel.gov/pv/cell-efficiency.html.
10 B. Ehrler, E. Alarcón-Lladó, S. W. Tabernig, T. Veeken, E. C. Garnett and A. Polman, Photovoltaics Reaching for the Shockley–Queisser Limit, *ACS Energy Lett.*, 2020, **5**, 3029–3033.
11 M. Jeong, I. W. Choi, E. M. Go, Y. Cho, M. Kim, B. Lee, S. Jeong, Y. Jo, H. W. Choi, J. Lee, J. H. Bae, S. K. Kwak, D. S. Kim and C. Yang, Stable perovskite solar cells with efficiency exceeding 24.8% and 0.3 V voltage loss, *Science*, 2020, **369**, 1615–1620.
12 G. Kim, H. Min, K. S. Lee, D. Y. Lee, S. M. Yoon and S. I. Seok, Impact of strain relaxation on performance of alpha-formamidinium lead iodide perovskite solar cells, *Science*, 2020, **370**, 108–112.

13 H. Lu, Y. Liu, P. Ahlawat, A. Mishra, W. R. Tress, F. T. Eickemeyer, Y. Yang, F. Fu, Z. Wang, C. E. Avalos, B. I. Carlsen, A. Agarwalla, X. Zhang, X. Li, Y. Zhan, S. M. Zakeeruddin, L. Emsley, U. Rothlisberger, L. Zheng, A. Hagfeldt and M. Gratzel, Vapor-assisted deposition of highly efficient, stable black-phase $FAPbI_3$ perovskite solar cells, *Science*, 2020, 370.

14 S. H. Turren-Cruz, A. Hagfeldt and M. Saliba, Methylammonium-free, high-performance, and stable perovskite solar cells on a planar architecture, *Science*, 2018, **362**, 449–453.

15 F. X. Xie, C. C. Chen, Y. Z. Wu, X. Li, M. L. Cai, X. Liu, X. D. Yang and L. Y. Han, Vertical recrystallization for highly efficient and stable formamidinium-based inverted-structure perovskite solar cells, *Energy Environ. Sci.*, 2017, **10**, 1942–1949.

16 M. I. Saidaminov, I. Spanopoulos, J. Abed, W. Ke, J. Wicks, M. G. Kanatzidis and E. H. Sargent, Conventional Solvent Oxidizes Sn(II) in Perovskite Inks, *ACS Energy Lett.*, 2020, **5**, 1153–1155.

17 Z. Chen, B. Turedi, A. Y. Alsalloum, C. Yang, X. Zheng, I. Gereige, A. AlSaggaf, O. F. Mohammed and O. M. Bakr, Single-Crystal $MAPbI_3$ Perovskite Solar Cells Exceeding 21% Power Conversion Efficiency, *ACS Energy Lett.*, 2019, **4**, 1258–1259.

18 Z. Chen, Q. Dong, Y. Liu, C. Bao, Y. Fang, Y. Lin, S. Tang, Q. Wang, X. Xiao, Y. Bai, Y. Deng and J. Huang, Thin single crystal perovskite solar cells to harvest below-bandgap light absorption, *Nat. Commun.*, 2017, **8**, 1890.

19 A. Y. Alsalloum, B. Turedi, X. Zheng, S. Mitra, A. A. Zhumekenov, K. J. Lee, P. Maity, I. Gereige, A. AlSaggaf, I. S. Roqan, O. F. Mohammed and O. M. Bakr, Low-Temperature Crystallization Enables 21.9% Efficient Single-Crystal $MAPbI_3$ Inverted Perovskite Solar Cells, *ACS Energy Lett.*, 2020, **5**, 657–662.

20 B. Turedi, V. Yeddu, X. Zheng, D. Y. Kim, O. M. Bakr and M. I. Saidaminov, Perovskite Single-Crystal Solar Cells: going Forward, *ACS Energy Lett.*, 2021, 631–642.

21 D. Shi, V. Adinolfi, R. Comin, M. Yuan, E. Alarousu, A. Buin, Y. Chen, S. Hoogland, A. Rothenberger, K. Katsiev, Y. Losovyj, X. Zhang, P. A. Dowben, O. F. Mohammed, E. H. Sargent and O. M. Bakr, Solar cells. Low trap-state density and long carrier diffusion in organolead trihalide perovskite single crystals, *Science*, 2015, **347**, 519–522.

22 Q. Dong, Y. Fang, Y. Shao, P. Mulligan, J. Qiu, L. Cao and J. Huang, Electron-hole diffusion lengths >175 μm in solution-grown CH3NH3PbI3 single crystals, *Science*, 2015, **347**, 967–970.

23 B. Murali, H. K. Kolli, J. Yin, R. Ketavath, O. M. Bakr and O. F. Mohammed, Single Crystals: the Next Big Wave of Perovskite Optoelectronics, *ACS Mater. Lett.*, 2019, **2**, 184–214.

24 K. Wang, D. Yang, C. Wu, J. Shapter and S. Priya, Monocrystalline Perovskite Photovoltaics toward Ultrahigh Efficiency?, *Joule*, 2019, **3**, 311–316.

25 B. M. Kayes, H. Nie, R. Twist, S. G. Spruytte, F. Reinhardt, I. C. Kizilyalli and G. S. Higashi, 27.6% Conversion efficiency, a new record for single-junction solar cells under 1 sun illumination, *IEEE Photovoltaic Spec. Conf., 34th*, 2011, 4–8.

26 Y. Liu, Y. Zhang, Z. Yang, D. Yang, X. Ren, L. Pang and S. F. Liu, Thinness- and Shape-Controlled Growth for Ultrathin Single-Crystalline Perovskite Wafers for Mass Production of Superior Photoelectronic Devices, *Adv. Mater.*, 2016, **28**, 9204–9209.

27 M. I. Saidaminov, A. L. Abdelhady, B. Murali, E. Alarousu, V. M. Burlakov, W. Peng, I. Dursun, L. Wang, Y. He, G. Maculan, A. Goriely, T. Wu, O. F. Mohammed and O. M. Bakr, High-quality bulk hybrid perovskite single crystals within minutes by inverse temperature crystallization, *Nat. Commun.*, 2015, **6**, 7586.

28 T. Baikie, Y. Fang, J. M. Kadro, M. Schreyer, F. Wei, S. G. Mhaisalkar, M. Graetzel and T. J. White, Synthesis and crystal chemistry of the hybrid perovskite $(CH_3NH_3)PbI_3$ for solid-state sensitised solar cell applications, *J. Mater. Chem. A*, 2013, **1**, 5628–5641.

29 M. I. Saidaminov, A. L. Abdelhady, G. Maculan and O. M. Bakr, Retrograde solubility of formamidinium and methylammonium lead halide perovskites enabling rapid single crystal growth, *Chem. Commun.*, 2015, **51**, 17658–17661.

30 X. Zheng, Y. Hou, C. Bao, J. Yin, F. Yuan, Z. Huang, K. Song, J. Liu, J. Troughton, N. Gasparini, C. Zhou, Y. Lin, D.-J. Xue, B. Chen, A. K. Johnston, N. Wei, M. N. Hedhili, M. Wei, A. Y. Alsalloum, P. Maity, B. Turedi, C. Yang, D. Baran, T. D. Anthopoulos, Y. Han, Z.-H. Lu, O. F. Mohammed, F. Gao, E. H. Sargent and O. M. Bakr, Managing grains and interfaces via ligand anchoring enables 22.3%-efficiency inverted perovskite solar cells, *Nat. Energy*, 2020, **5**, 131–140.

31 S. Akin, N. Arora, S. M. Zakeeruddin, M. Grätzel, R. H. Friend and M. I. Dar, New Strategies for Defect Passivation in High-Efficiency Perovskite Solar Cells, *Adv. Energy Mater.*, 2020, **10**, 1903090.

32 D. Luo, R. Su, W. Zhang, Q. Gong and R. Zhu, Minimizing non-radiative recombination losses in perovskite solar cells, *Nat. Rev. Mater.*, 2019, **5**, 44–60.

33 L. Fu, H. Li, L. Wang, R. Yin, B. Li and L. Yin, Defect passivation strategies in perovskites for an enhanced photovoltaic performance, *Energy Environ. Sci.*, 2020, **13**, 4017–4056.

34 X. Lin, D. Cui, X. Luo, C. Zhang, Q. Han, Y. Wang and L. Han, Efficiency progress of inverted perovskite solar cells, *Energy Environ. Sci.*, 2020, **13**, 3823–3847.

35 L. Krückemeier, U. Rau, M. Stolterfoht and T. Kirchartz, How to Report Record Open-Circuit Voltages in Lead-Halide Perovskite Solar Cells, *Adv. Energy Mater.*, 2019, **10**, 1902573.

36 Q. Jiang, Y. Zhao, X. Zhang, X. Yang, Y. Chen, Z. Chu, Q. Ye, X. Li, Z. Yin and J. You, Surface passivation of perovskite film for efficient solar cells, *Nat. Photonics*, 2019, **13**, 460–466.

37 Y. Liu, Q. Dong, Y. Fang, Y. Lin, Y. Deng and J. Huang, Fast Growth of Thin MAPbI3 Crystal Wafers on Aqueous Solution Surface for Efficient Lateral-Structure Perovskite Solar Cells, *Adv. Funct. Mater.*, 2019, **29**, 1807707.

38 Y. Song, W. Bi, A. Wang, X. Liu, Y. Kang and Q. Dong, Efficient lateral-structure perovskite single crystal solar cells with high operational stability, *Nat. Commun.*, 2020, **11**, 1–8.

